

Pushing the Limit of Phase Shift Feedback Compression for Intelligent Reflecting Surface-Assisted Wireless Systems by Exploiting Global Attention

Xianhua Yu, Dong Li *senior member, IEEE*,

Abstract—Intelligent reflecting surface (IRS) has recently appeared as a potential technology for 6G, and received much attention from academia and industry. However, most of existing works on IRS focus on how to compute the phase shift for performance enhancement, and the problem on how to obtain the computed phase shift at the IRS side is generally neglected. In this paper, we consider compressing the computed phase shift at the receiver side to the IRS through a bandwidth-limited feedback channel. In particular, we propose and investigate a novel attention mechanism named as global attention by exploiting the attention map over both spatial and channel dimensions. This allows us to push the limit of phase shift feedback compression by utilizing the two-dimensional information, which is in sharp contrast to existing works that only consider either the spatial or channel dimension. Besides, to cope with the problem of mismatched distribution of the phase shift, we introduce the generalized divisive normalization (GDN) layer and inverse generalized divisive normalization (IGDN) layer to the proposed global attention phase shift compression network (GAPSCN). Furthermore, due to practical constraints on the IRS, it is desirable to consider a simplified GAPSCN (S-GAPSCN), where a lightweight multi-scale simplified global attention module (MSSGAM) is proposed in the decoder located at the IRS side to compensate for the performance degradation due to the simplified structure. Simulation results show that the proposed GAPSCN is able to achieve a reconstruction accuracy close to 1 and performs much better than existing algorithms. The performance of the proposed S-GAPSCN can approach that of the GAPSCN but with a much lower computational load.

Index Terms—Intelligent reflecting surface, feedback compression, global attention, convolutional neural network.

I. INTRODUCTION

The intelligent reflecting surface (IRS), as a promising wireless innovation with the development of microelectromechanical systems (MEMS) and metamaterial, has recently attracting much attention in wireless communications and Internet of Things (IoT) [1] and [2]. The IRSs are two-dimensional man-made surfaces with low-cost passive reflecting elements with adjustable phases that are connected to base station (BS)/access points (APs) through a smart controller. In particular, the reflecting elements (e.g., printed dipoles) passively reflect the impinging signals with no need for radio frequency (RF) chains, such that they can be implemented/managed with orders-of-magnitude lower hardware/energy costs compared

to traditional active antenna arrays. Moreover, since IRS is generally characterized by the low profile, lightweight, and conformal geometry, it can be easily mounted on/removed from environment objects for deployment or replacement. Furthermore, IRS can serve as an auxiliary device in wireless networks and can be easily integrated into them, thus providing great flexibility and compatibility with existing wireless systems (e.g., cellular or WiFi).

In the IRS-assisted wireless system, it is crucial to control the phase of the reflection elements to ensure an optimized performance. Many studies have been conducted to determine optimal/suboptimal phases based on different optimization objectives (see, e.g., [3]–[6]). However, most existing works assume the IRS is fully aware of the quantized phase shift (QPS). It is in fact difficult to obtain QPS on the IRS side due to practical limits on bandwidth and data rates in feedback channels. This problem is neglected in existing works except our previous work [7]. In our previous work [7], we addressed this issue by proposing an autoencoder-based neural network model named phase shift compression and denoising network (PSCDN), which compresses the QPS in the encoder at the receiver side and reconstructs it in the decoder at the IRS side.

On the other hand, the attention mechanism [8] has developed into an increasingly significant component of computer vision over the last decade. In the previous works [9]–[14], various attention mechanisms have been developed. The squeeze-and-excitation (SE) networks [11] was proven to be one of the most popular methods for processing attention with a convolutional operation. SE networks was succeeded by the convolutional block attention module (CBAM) [12], which emphasized providing robust representative attention by incorporating spatial attention and channel attention. The CBAM incorporates dimensionality reduction in computing channel attention which is redundant to capture nonlinear local dependencies between the channels. Different from traditional SE block process the 'squeeze' operation by utilizing the global average pooling (GAP) operation, the tiled squeeze-and-excite (TSE) block used the average pooling to run efficiently on common AI accelerators with data flow design [13]. In addition, the numerical results showed that channel attention learned with local spatial context performed a comparable performance than learned with global spatial context [13]. By using a triplet attention [14] approach, the redundancy was

Xianhua Yu, Dong Li are with the School of Computer Science and Engineering, Macau University of Science and Technology, Macau 999078, China (e-mails: 2009853gii30014@student.must.edu.mo; dli@must.edu.mo).

minimized, which accounted for cross-dimension interaction efficiently. triplet attention is comprised of three branches, each of which is responsible for capturing cross-dimensional relations between spatial and channel dimensions. The convolutional neural networks (CNN) generate multiple output feature maps by a convolution between the same input feature map and multiple kernels [15]. With the same input feature map as input, it is highly possible that each of the output feature maps, along with the channel dimension, are correlated with each other. In other words, the channel dimension information may be related with the spatial dimension information. However, previous attention-based studies calculated the attention map along channels and spatial dimensions separately and there has no research effort that has been paid to utilize the joint channel dimension and spatial dimension information. To this end, it is interesting to calculate a joint channel and spatial attention map in addition to the conventional attention module which could enhance the model’s performance.

However, a natural question arises: is it possible to push the limit of phase shift feedback compression by using the attention mechanism? To this end, in this paper, we propose an attention-based neural network named global attention phase shift compression network (GAPSCN) in this paper. GAPSCN consists of a novel global attention module, generalized divisive normalization (GDN) layers, and inverse generalized divisive normalization (IGDN) layers [16] to enhance the overall performance and resolve the issue of mismatch distributions. Specifically, the GAPSCN-encoder stochastically maps the QPS information at the receiver side to a code with a smaller dimension in the feature space and sends it to the IRS side via a feedback channel. By learning to decode the corrupted code with noise, the GAPSCN-decoder is able to reconstruct the original QPS information. The contributions of this paper are summarized as follows:

- We propose a novel global attention module that emphasizes information not only along with the channel and the spatial dimension separately, but also globally emphasizes the channel dimension information and spatial dimension information jointly. In contrast to previous attention-based studies, here we avoid using average pooling and maximum pooling layer in global attention module, which captures more detailed information.
- We further propose a simplified GAPSCN (S-GAPSCN) in which the architecture of the decoder is much simpler than that of the encoder. Specifically, to compensate for the performance degradation caused by simplifying the model, we propose a lightweight multi-scale simplified global attention module (MSSGAM) in the decoder of S-GAPSCN. The MSSGAM aims to suppress the additive white Gaussian noise (AWGN) effect by adopting a structure of multi-scale and simplified global attention.
- Simulation results show that the proposed global attention outperforms the existing attention mechanism by adding the missing joint channel-spatial attention map and capturing more crucial information by abandoning the pooling layer. Furthermore, our proposed GAPSCN achieves significant reliability in the reconstruction ac-

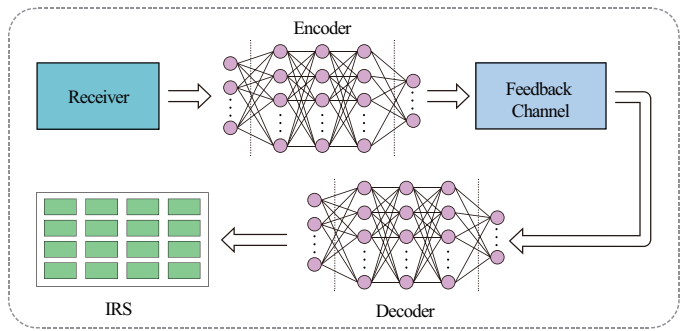


Fig. 1. An IRS-assisted wireless system with feedback compression.

curacy compared to existing algorithms by solving the mismatch distribution with the GDN layer and capturing more important information with the global attention module. Besides, the S-GAPSCN assisted by MSSGAM offers impressive performance at a relatively low computational cost.

It should be noted that this work is significantly different from traditional attention-based compression techniques (see, e.g. [17], [18]) due to the two novel modules (i.e., global attention module and MSSGAM). Besides, in most of previous works in wireless communications, the channel state information (CSI) was considered for feedback, but with a feedback overhead that is proportional to the number of transmit antennas. The feedback of the QPS in this study does not suffer from this problem which only depends on the number of reflecting elements and quantization levels (as described in the next section). Besides, it is worth pointing out that our propose feedback compression method is applicable to all kinds of wireless systems where the QPS is available at the receiver side.

The remainder of this paper is organized as follows. Section II illustrates the system model. In section III, we briefly discuss the global attention and the architecture of GAPSCN. An asymmetric model, S-GAPSCN, is presented in section IV. In section V, we provide details regarding the training procedure, simulation results, and an analysis of the simulation results. In section VI, we conclude this paper. The abbreviations in this paper are given by Table I.

II. SYSTEM MODEL

In this paper, we consider the feedback compression from the receiver to the IRS to deliver the QPS, as shown in Fig. 1, where the IRS is equipped with M reflecting elements ($\forall m \in \mathcal{M} = \{1, 2, \dots, M\}$). Due to the finite resolution of the IRS, the phase shift for the m -th reflecting element θ_m can only take a finite number of discrete values (see, e.g., [19] [20].) i.e., 2^K quantization levels and K denotes the number of quantization bits. Moreover, θ_m can be uniformly quantized and the set of QPS is given by $\left\{0, \frac{2\pi}{2^K}, \dots, \frac{(2^K-1)2\pi}{2^K}\right\}$. Thus, θ_m can be represented by K bits by using, for instance, the phase shift keying (PSK) mapping.

By designing an autoencoder [21], as illustrated in Fig. 1, we intend to reduce the feedback overhead for the QPS. The autoencoder is composed of two components: an encoder and

TABLE I
ABBREVIATIONS

| Notation | Meaning |
|----------|---|
| 1D | One dimensional |
| 2D | Two dimensional |
| 3D | Three dimensional |
| AP | Access point |
| AWGN | Additive white Gaussian noise |
| BS | Base station link |
| CARB | Compression attention residual block |
| CBAM | Convolutional block attention module |
| CNN | Convolutional neural networks |
| CR | Compression ratio |
| CRB | Compression residual block |
| CSI | Channel state information |
| FC | Fully connected |
| GAP | global average pooling |
| GAPSCN | Global attention phase shift compression network |
| GDN | Generalized divisive normalization |
| GMP | Global max pooling |
| IGDN | Inverse generalized divisive normalization |
| IoT | Internet of Things |
| IRS | Intelligent reflecting surface |
| MEMS | microelectromechanical system |
| MLP | Multilayer perceptron |
| MSE | Mean squared error |
| MSSGAM | Multi-scale simplified global attention module |
| PSCDN | Phase shift compression and denoising network |
| PSK | Phase shift keying |
| QPS | Quantized phase shift |
| RARB | Reconstruction attention residual block |
| RB | Residual block |
| RF | Radio frequency |
| RRB | Reconstruction residual block |
| SE | Squeeze-and-excitation |
| S-GAPSCN | Simplified global attention phase shift compression network |
| TSE | Tiled squeeze-and-excite |

a decoder [21]. In an encoder, an input value x is stochastically mapped to the feature space and a code value c is produced $c = f(x)$. While in the decoder, the estimated input \hat{x} is reconstructed from a feature space code c i.e., $\hat{x} = g(c)$. Thus, the encoder learns to map $\Theta = [\theta_1, \theta_2, \dots, \theta_M]$ to a code (with low-dimension), and the decoder learns to reconstruct x from c . In particular, the encoding and decoding processes are specified by $C = f(\Theta)$ and $\hat{\Theta} = g(C)$, where C represents the code in the feature space.

III. GLOBAL ATTENTION PHASE SHIFT COMPRESSION NETWORK

In this section, we begin with the review of conventional attention mechanisms, and proceed with the introduction of our proposed global attention mechanism. Specifically, we will briefly describe the architecture of the proposed GAPSCN and compare its performance with existing attention mechanisms according to the mean square function and the accuracy function based on Tensorflow [22].

A. Existing Attention mechanisms

As a first step in our explanation of global attention, let us review previous attention modules, i.e., SE block [11], CBAM [12], TSE block [13] and triplet attention [14], which are illustrated in Fig. 2(a), Fig. 2(b), Fig. 2(c) and Fig. 2(d), respectively.

1) *SE block*: The SE block compute the attention map AM by utilizing a GAP to capture the channel-wise information and a fully connected (FC) layer to reduce the computational complexity followed by a nonlinear activation function ReLU. Then, it uses a FC layer to reconstruct the original dimension, and a sigmoid function used for nonlinear transformation of the information to interval $[0, 1]$. At last, the attention process computes the element-wise product of the input and the attention map. The attention is computed as:

$$\begin{aligned} AM_{se} &= \sigma(f_{fc}(f_{ReLU}(f_{fc}((f_{GAP}(X)))))) \\ ATT_{se} &= X \otimes AM_{se} \end{aligned} \quad (1)$$

where X , σ , \otimes , f_{fc} , f_{ReLU} and f_{GAP} denote the input, the sigmoid function, element-wise product, fully connect layer, nonlinear activation function ReLU and GAP operation, respectively.

2) *CBAM*: The CBAM consists of two modules, one for channel attention and the other for spatial attention. By using GAP and global max pooling (GMP), channel attention produces two spatial features. Then, two features are forwarded to a multilayer perceptron (MLP) with one hidden layer, and the output features are then merged using the element-wise summation. Let AM_c be the channel attention map produced by applying a sigmoid function to the summation feature. The channel attention is computed as:

$$\begin{aligned} AM_c &= \sigma(f_{MLP}(f_{GAP}(X)) + f_{MLP}(f_{GMP}(X))) \\ ATT_c &= X \otimes AM_c \end{aligned} \quad (2)$$

where f_{MLP} and f_{GMP} denote the MLP layer and GMP operation, respectively.

Different from channel attention, the two spatial features are concatenated together and then forwarded to a convolutional layer to produce the spatial attention map AM_s . The spatial attention is computed as:

$$\begin{aligned} AM_s &= \sigma(f_{BN}((f_{1 \times 1}([f_{GAP}(Att_c); f_{GMP}(Att_c)])))) \\ ATT_s &= ATT_c \otimes AM_s \end{aligned} \quad (3)$$

where f_{BN} and $f_{1 \times 1}$ denote the batch normalization layer and convolutional layer with a kernel of size 1×1 , respectively.

3) *TSE block*: The only difference between traditional SE block and TSE block is the structure of the 'squeeze'. Different from traditional SE block using a GAP, the TSE block utilizes a average pooling with a pooling size (h,w) to run efficiently on common AI accelerators with data flow. The attention map calculates in the TSE block by a average pooling layer, a convolutional layer with a nonlinear activation function ReLU, a convolutional layer with a nonlinear activation function sigmoid and a nearest-neighbor interpolation. The attention is computed as:

$$\begin{aligned} AM_{tse} &= f_{nnp}(\sigma(f_{1 \times 1}(f_{ReLU}(f_{1 \times 1}(f_{ap}(X)))))) \\ ATT_{tse} &= X \otimes AM_{tse} \end{aligned} \quad (4)$$

where f_{nnp} and f_{ap} denote the nearest-neighbor interpolation and the average pooling operation, respectively.

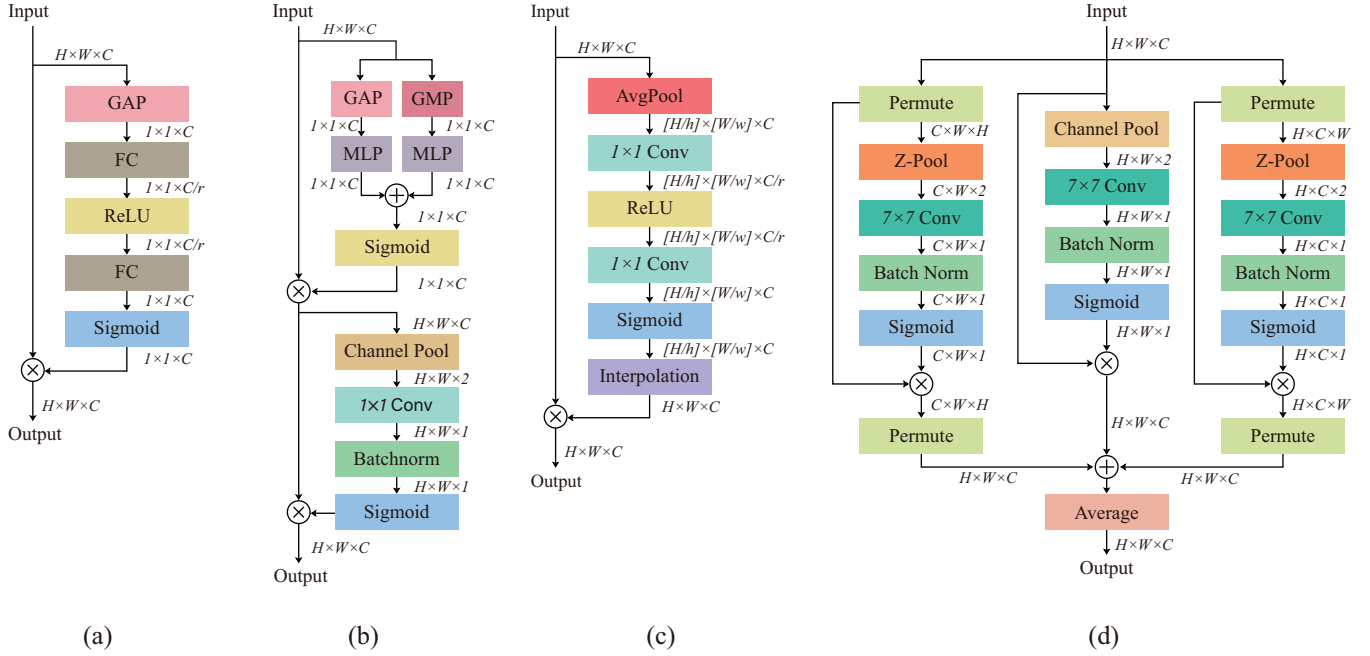


Fig. 2. Comparison with different attention modules: (a) SE block; (b) CBAM; (c) TSE block; (d) Triplet attention; 1×1 Conv, 7×7 Conv denote convolutional layer with a kernel of size 1×1 and 7×7 , respectively. The operation of channel pool and z-pool process a GAP and a GMP to the last dimension of the input, respectively, and concat the output along the last dimension.

4) *Triplet Attention*: This approach consists of three branches: the first and the third branches are similar to spatial attention in CBAM except a rotation operation added to the beginning of both branches; while the second branch is a direct equivalent to the spatial attention in CBAM. The final step involves applying a simple average operation to the output of three branches. The triplet attention can be computed as:

$$\begin{aligned}
 AM_{ta1} &= \sigma(f_{7 \times 7}([f_{GAP}(f_{Rt}(X)); f_{GMP}(f_{Rt}(X))])) \\
 ATT_{ta1} &= f_{Rt}(f_{Rt}(X) \otimes AM_{ta1}) \\
 AM_{ta2} &= \sigma(f_{7 \times 7}([f_{GAP}(f_{Rt}(X)); f_{GMP}(f_{Rt}(X))])) \\
 ATT_{ta2} &= f_{Rt}(f_{Rt}(X) \otimes AM_{ta2}) \\
 AM_{ta3} &= \sigma(f_{7 \times 7}([f_{GAP}(F); f_{GMP}(X)])) \\
 ATT_{ta3} &= X \otimes AM_{ta3} \\
 ATT_{ta} &= \frac{1}{3}(Att_{ta1} + Att_{ta2} + Att_{ta3})
 \end{aligned} \tag{5}$$

where $f_{1 \times 1}$ and f_{Rt} denote the convolutional layer with a kernel of size 7×7 and the operation of permutation, respectively.

B. Motivation of GAPSCN

The output feature maps in a CNN are generated by a convolution between the input feature map and multiple kernels. With the same input feature map, each of the output feature maps along with the channel dimension in the CNN, should be correlated with each other. In other words, there may exist a correlation between the channel dimension information and the spatial dimension information.

In most previous attention-based works, the crucial information has been emphasized along two dimensions separately:

channel dimension (what is the meaningful information necessary to be paid attention to) and spatial dimension (where is the meaningful information necessary to be paid attention to). However, channel dimension and spatial dimension are generally considered separately in previous works when processing the attention map, where the correlation between the channel dimension and the spatial dimension is neglected and thus the joint information acquisition is missing.

Based on this observation, we propose a novel global attention to capture the joint information, which produces attention maps not only across the channel dimension or the spatial dimension separately but also the joint channel dimension and spatial dimension globally. Furthermore, we abandon the pooling operation in the global attention, unlike previous attention modules which were composed of an average-pooling layer and a max-pooling layer. The previous works focused on the processing of image data accompanied by a large primary object that requires attention, which is helpful for capturing this primary object. As opposed to image data which has one or more primary objects, each bit in the QPS is crucial for the phase adjustment in the IRS, which means that each bit is equal in weight, and it is impossible to use the pooling operation to obtain highly-weighted information. Rather than using a pooling operation to deal with the case where each bit has an equal weight, we use the convolutional layer with a kernel of size 1 in order to save more detailed information and get a feature map. In the following section, we will examine the ablation study of the information replenishment and the removal of the pooling.

The architecture of global attention is shown in Fig. 3, which is composed of three components; the first computes the attention map along the spatial dimension by means of a

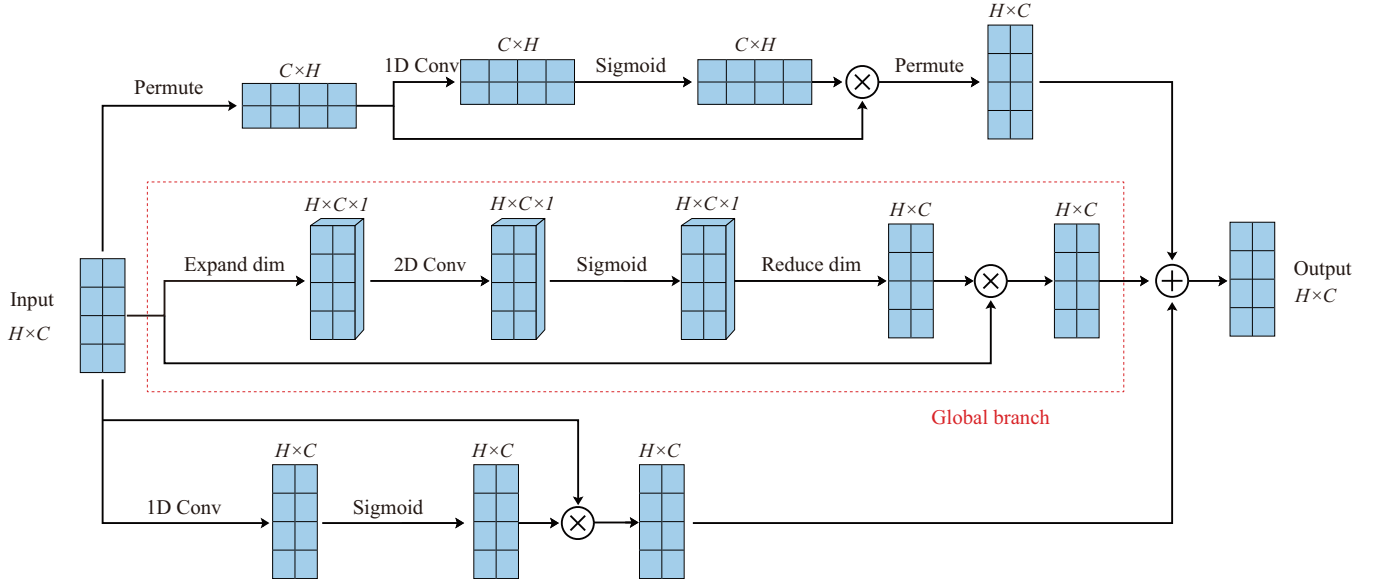


Fig. 3. The architectures of the global attention. Expand dim and Reduce dim denote the operation of expanded dimension and the operation of reduced dimension, respectively.

one-dimensional (1D) convolutional layer with a kernel of size 1, and the output feature map is subject to signal processing by utilizing a non-linear activation function (sigmoid); the second branch computes attention along the channel dimension by combining a permutation layer, a 1D convolutional layer with a kernel of size 1, and a nonlinear sigmoid function. Following the operation of an element-wise product between attention map input and rotate dimension input, we rotate the output dimension to the origin input dimension. In the third branch, in order to consider channel dimension and spatial dimension as a whole, we expand one null dimension to input (e.g. the input dimension is $H \times C$ and the output by the expansion operation is $H \times C \times 1$). Following that, we use a two-dimensional (2D) convolutional layer with kernel size 1×1 and nonlinear activation function sigmoid to compute the attention map. As we need to keep the dimension of the attention map consistent, we apply the squeeze dimension operation before applying the element-wise product between the attention map and the expand dimension input. By doing so, the global attention captures dependencies between the (C, H) , (H, C) , and $(H \times C, H \times C)$ dimensions of the input, respectively. Last but not least, to gain comprehensive attention, we aggregate the outputs of each branch. We formulate the global attention as follows:

$$\begin{aligned}
 AM_{ga1} &= \sigma(f_1(f_{Rt}(X))) \\
 ATT_{ga1} &= f_{Rt}(X) \otimes AM_{ga1} \\
 AM_{ga2} &= \sigma(f_{rd}(f_{1 \times 1}(f_{ep}(X)))) \\
 ATT_{ga2} &= f_{ep}(X) \otimes AM_{ga2} \\
 AM_{ga3} &= \sigma(f_1(X)) \\
 ATT_3 &= X \otimes AM_{ga3} \\
 ATT_{ga} &= ATT_{ga1} + ATT_{ga2} + ATT_{ga3}
 \end{aligned} \tag{6}$$

where f_1 , f_{ep} and f_{rd} denote the convolutional layer with a kernel of size 1, the operation of the expanded dimension and

the operation of the reduced dimension, respectively.

C. Architecture of GAPSCN

The architecture of GAPSCN is shown in Fig. 4, which is composed of an encoder and a decoder. The encoder is comprised of multiple compression attention residual blocks (CARBs), one convolutional layer, and one GDN layer, while the decoder is comprised of multiple reconstruction attention residual blocks (RARBs) and one convolutional layer. (The number of CARB and RARB depends on the compression rate (CR). (For instance, GAPSCN with $CR = \frac{1}{8}$ has three CARBs and three RARBs).

In Fig. 4, GDN is defined in terms of an inevitable nonlinear transformation that is optimized so as to Gaussianize the data. The transformation process is given by

$$y_i = \frac{z_i}{(\beta_i + \sum_j \gamma_{ij} |z_j|^{\alpha_{ij}})^{\epsilon_i}} \tag{7}$$

$$z_i = Hx_i. \tag{8}$$

where x is input vector, β, ϵ are vector parameters, α, γ are matrix parameters. The GDN transformation can be efficiently inverted using a fixed point iteration. The GDN/IGDN is an efficient algorithm for fitting the parameters of this transformation, minimizing the Kullback-Leibler divergence of the distribution of transformed data against a Gaussian target, which preserves a better information than ReLU.

The CARB is composed of the compression residual blocks (CRBs), followed by the residual blocks (RBs), a global attention module, and one GDN layer. As shown in Fig. 4, the CRB is made up of two branches: the first branch is composed of a convolutional layer followed by a downsampling layer (max pooling). The second branch consists of a convolutional layer followed by a downsampling layer and a convolutional layer. The output of each branch is then combined. The last step involves transforming the input distribution into a

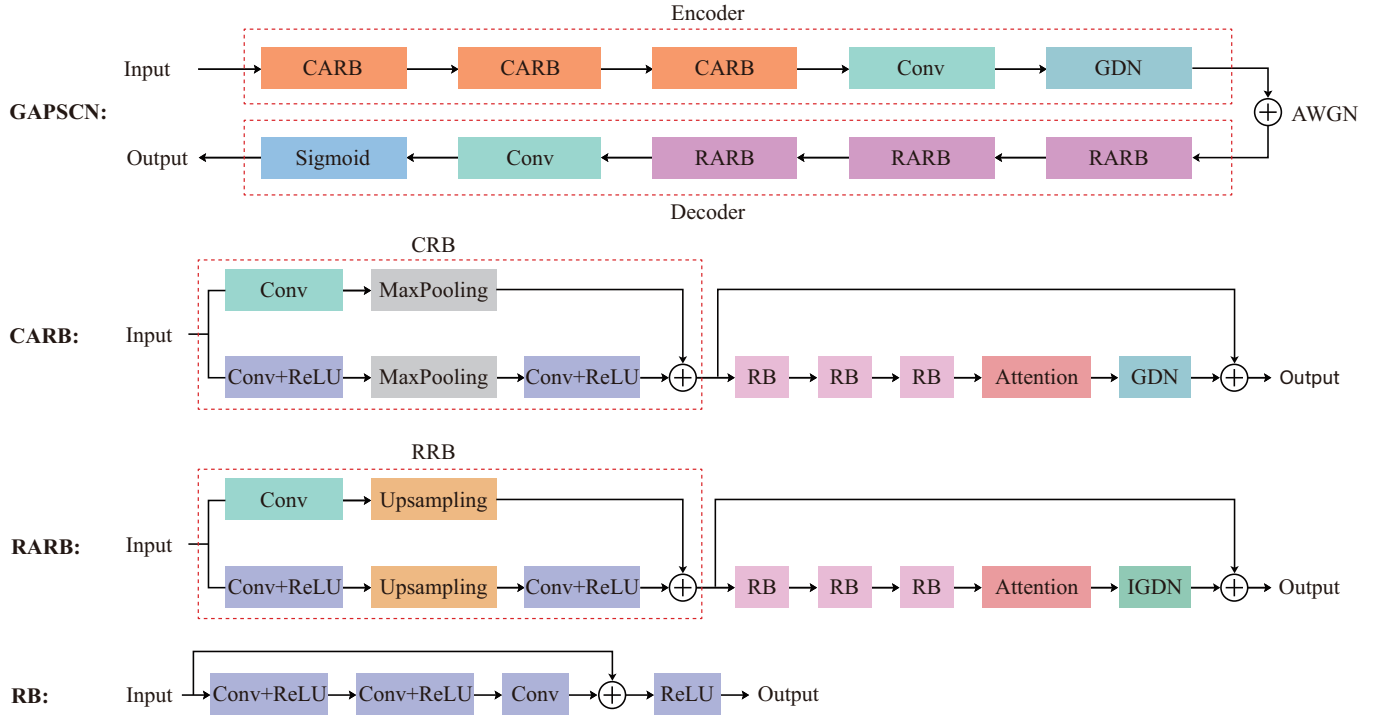


Fig. 4. The architectures of the GAPSCN.

Gaussian distribution using a GDN layer. Based on the success in [23], we apply three RBs to capture deep information before the attention module. Every RB consists of a 1D convolutional layer with a kernel of size 1, followed by a 1D convolutional layer with a kernel of size 3, and finally a 1D convolutional layer with a kernel of size 1. At the end of the RB, a residual add operation is applied between the input and output of the last convolutional layer. By utilizing the GDN layer, the output of the attention module will be converted to a Gaussian distribution. Last, we add the output of the RBs and the output of the GDN layer for a fast convergence [24].

The RARB is composed of a reconstruction residual block (RRB), three RBs, a global attention module, and an IGDN layer. As shown in Fig. 4, the RRB is almost equivalent to the CRB, the main difference is that the downsampling layer is switched for an upsampling layer (double input along the first dimension) and the IGDN layer is used to transform the Gaussian distribution back to the original uniform distribution. To capture the deep information of reconstructed features, we use three RBs similar to CARB. In the following step, we convert the output of the attention module to the original input distribution by utilizing the IGDN layer. Last but not least, in RARB, the RBs and the IGDN layer outputs will be combined for a fast convergence [24].

The CARB's output will go through a convolutional layer with a kernel of size 1 and a filter of size 1 to reduce the dimension of the channel to 1. Thereafter, a GDN layer is applied to transform the uniform data distribution to Gaussian distribution. The output of a RARB will go through a convolutional layer with a kernel of size 1 and a filter of size 1 and is activated by a nonlinear function sigmoid in the decoder in order to reconstruct the QPS. A comprehensive view of

TABLE II
SHAPE OF EACH INPUT/OUTPUT OF EACH LAYER/BLOCK

| Layer/Block | Input shape | Output shape |
|----------------|-----------------|-----------------|
| Encoder | | |
| CARB | 128×1 | 64×64 |
| CARB | 64×64 | 32×64 |
| CARB | 32×64 | 16×64 |
| GDN | 16×64 | 16×64 |
| Conv | 16×64 | 16×1 |
| GDN | 16×1 | 16×1 |
| Decoder | | |
| RARB | 16×1 | 32×64 |
| RARB | 32×64 | 64×64 |
| RARB | 64×64 | 128×64 |
| IGDN | 128×64 | 128×64 |
| Conv | 128×64 | 128×1 |
| Sigmoid | 128×64 | 128×1 |

GAPSCN can be obtained by noting the input/output shape of each layer as shown in Table II.

D. Performance comparison and ablation study

To determine the relative effectiveness of different attention modules, we chose the GAPSCN as the basic architecture and trained it by switching between different attention modules. In addition, we conduct three ablation studies here to study the effect of the GDN/IGDN layer, global branch, and pool operations. We only chose the triplet attention and the TSE block as the comparison candidates since triplet attention already outperforms CBAM, and TSE block outperforms SE block. The CBAM combined with attention CsiNet [17] and the modified SE block combined with SALDR [18] will be compared with proposed GAPSCN in Section VI. Due to the

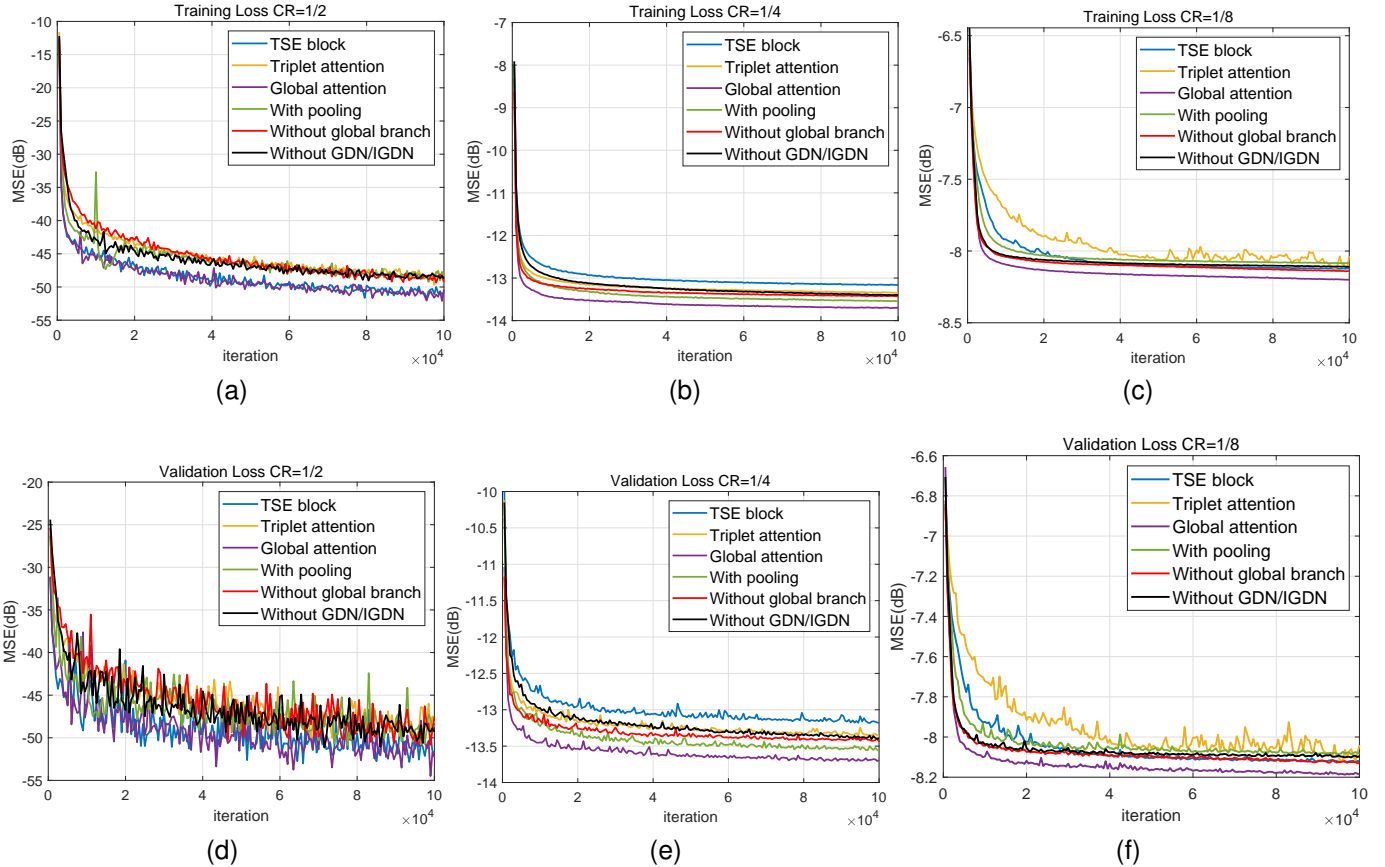


Fig. 5. Training Loss and Validation Loss of GAPSCN + various attention mechanisms (global attention, global attention without global branch, TSE block and triplet attention) and GAPSCN without GND/IGDN layer under different CR. (a) Training accuracy under $CR = \frac{1}{2}$. (b) Training accuracy under $CR = \frac{1}{4}$. (c) Training accuracy under $CR = \frac{1}{8}$. (d) Validation accuracy under $CR = \frac{1}{2}$. (e) Validation accuracy under $CR = \frac{1}{4}$. (f) Validation accuracy under $CR = \frac{1}{8}$.

TABLE III
TRAINING ACCURACY AND VALIDATION ACCURACY

| Type of Module | $CR = \frac{1}{2}$ | | $CR = \frac{1}{4}$ | | $CR = \frac{1}{8}$ | |
|------------------------|--------------------|----------------|--------------------|----------------|--------------------|----------------|
| | Training acc | Validation acc | Training acc | Validation acc | Training acc | Validation acc |
| TSE block [11] | 0.999992 | 0.999994 | 0.9307 | 0.9309 | 0.756 | 0.756 |
| Triplet attention [14] | 0.999986 | 0.999988 | 0.9353 | 0.9354 | 0.752 | 0.752 |
| Global attention | 0.999992 | 0.999995 | 0.9409 | 0.9410 | 0.768 | 0.768 |
| With pooling | 0.999985 | 0.999990 | 0.9385 | 0.9389 | 0.766 | 0.766 |
| Without global branch | 0.999986 | 0.999990 | 0.9368 | 0.9369 | 0.765 | 0.764 |
| Without GDN/IGDN | 0.999985 | 0.999991 | 0.9354 | 0.9353 | 0.763 | 0.762 |

1D nature of input data, the 2D convolutional layer in each attention module will be converted to a 1D convolutional layer. We will elaborate the parameter settings as well as the training procedure in Section VI.

As shown in Fig. 5, the training and validation losses for different attention mechanisms are illustrated (global attention, global attention without pooling layer, global attention without the global branch, TSE block and triplet attention) as well as GAPSCN without GND/IGDN layer under the conditions of $CR \in [\frac{1}{2}, \frac{1}{4}, \frac{1}{8}]$. With an increasing CR, the training loss and validation loss of each model are decreasing. Across all CRs, it is found that global attention is superior both in terms of training loss and validation loss, demonstrating the effectiveness of correlated information replenishment. In the absence of pooling operation, more critical information

is preserved in the global attention, resulting in a better performance of the global attention compared with that with pooling. By overcoming the mismatch distribution problem, the compression performance can be improved. It has been demonstrated that GAPSCN with GND/IGDN layers achieves a much lower training loss and validation loss than GAPSCN without GND/IGDN layers.

To further evaluate the performance, we select the accuracy function provided by TensorFlow. The training accuracy and validation accuracy of each model are presented in Table III. The global attention achieves the highest training accuracy and corresponding validation accuracy in each CR, with a similar fashion to the trends in training loss and validation loss. All three ablation studies show trends that are similar to mean squared error (MSE) results, demonstrating that the

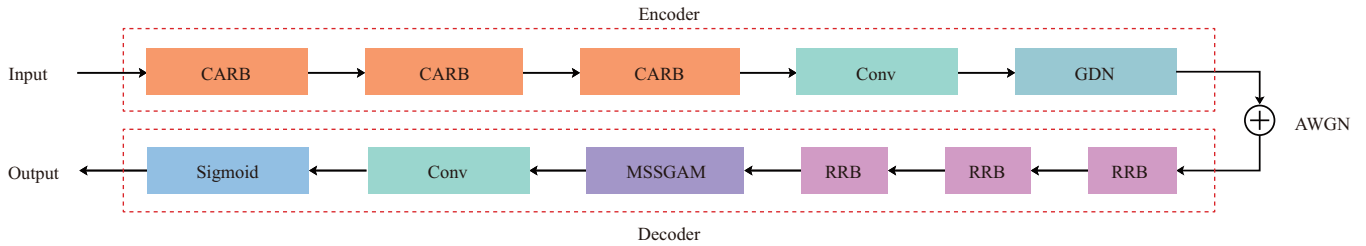


Fig. 6. The architectures of the S-GAPSCN.

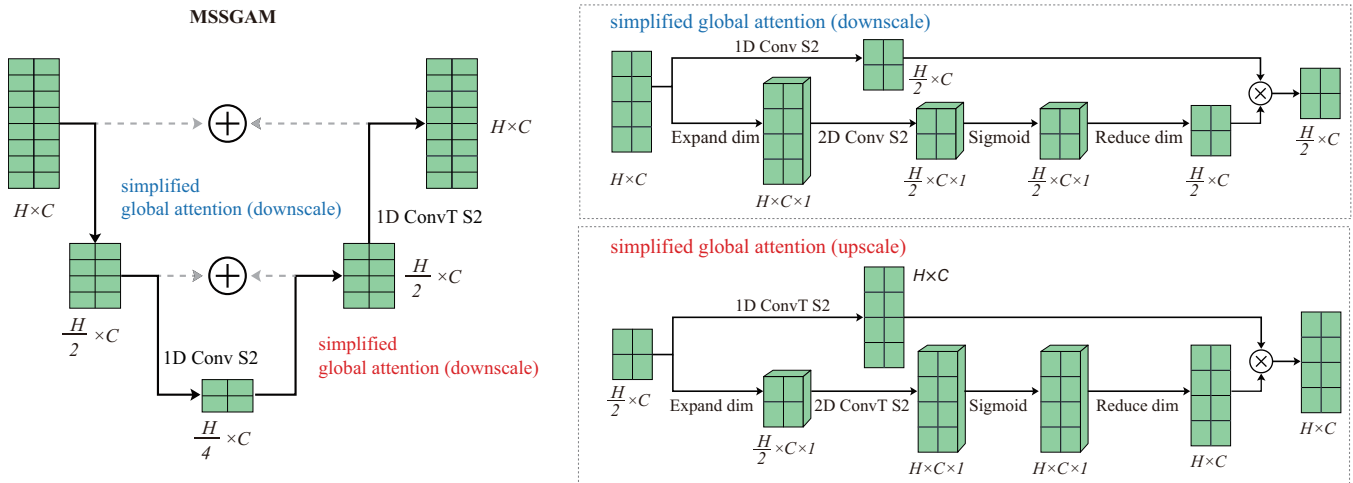


Fig. 7. The architectures of the SGAPSCN, simplified global attention (upscale) and simplified global attention (downscale). The S2 in MSSGAM stand for the convolutional layer or transpose convolutional layer with stride 2.

modification made in the proposed GAPSCN is beneficial to enhance the performance.

IV. SIMPLIFIED GLOBAL ATTENTION PHASE SHIFT COMPRESSION NETWORK

Recall GAPSCN has a symmetric structure regarding the encoder and the decoder as shown in Fig. 4, and thus resulting in an (almost) equal hardware complexity. However, this may not be always applicable to the IRS due to the practical constraints including the size, the cost and/or the power consumption. In this section, we propose and investigate the S-GAPSCN whose computational complexity of the decoder is significantly lower than that of the encoder.

A. Architecture of S-GAPSCN

Features scaling architectures (e.g., downscale and upscale) have achieved tremendous success in image processing, including the well-known u-net [25] adopted for 2D biomedical image segmentation, three-dimensional (3D) image segmentation [26], and image restoration [27]–[29]. In addition, there is increasing attention that has been paid to image denoising by using feature scaling architectures such as [30]–[33]. In contrast to aforementioned works, an attention guided scaling network for accurate image denoising was investigated in [33], which employed channel attention and spatial attention in multi-scale operation to enhance the denoising performance.

TABLE IV
PERFORMANCE OF MSE AND ACCURACY

| CR | Method | Simplified global attention | CS attention [33] |
|--------------------|----------|-----------------------------|-----------------------|
| $CR = \frac{1}{2}$ | MSE | 6.34×10^{-6} | 5.97×10^{-5} |
| | Accuracy | 0.99999 | 0.99992 |
| $CR = \frac{1}{4}$ | MSE | 0.0446 | 0.0513 |
| | Accuracy | 0.9369 | 0.9316 |
| $CR = \frac{1}{8}$ | MSE | 0.1535 | 0.1628 |
| | Accuracy | 0.7611 | 0.7604 |

It is noted that the above solutions are not suitable for S-GAPSCN since two attention processes are associated which incur a high computational cost.

Inspired by the success of feature scaling architectures in image processing, we propose a lightweight MSSGAM to compensate for the performance degradation caused by simplifying the model size of the decoder, which is shown in Fig. 7. The details of MSSGAM are shown in Fig. 7, which consist of two downscale processes (the first with attention mechanisms) and two upscale processes (the first with attention mechanisms). Similar to [33], we use a convolutional layer with stride 2 to downscale the data and a transpose convolutional layer with stride 2 to upscale the data. It should be noted that the attention downscale process consists of two branches. The first branch generates the attention map by adopting the simplified global attention which expands one dimension for features and employs a 2D convolutional layer with a nonlinear activation function sigmoid to produce the attention map and

reduce the expanded dimension to obtain the final attention map. The second branch uses the convolutional layer to extract the most important information from input data. In the end, we construct an element-wise product between the outputs of the two branches. There is only one difference between the upscale and downscale processes: we change the 2D convolutional layer to a 2D transpose convolutional layer for the upscale process, while there is no such change for the downscale process. The MSSGAM can be formulated as follows:

$$\begin{aligned}
AM_D &= \sigma(f_{rd}(f_{2dConv}(f_{ep}(X)))) \\
ATT_D &= f_{2dConv}(X) \otimes AM_D \\
AM_U &= \sigma(f_{rd}(f_{2dTCConv}(f_{ep}(X)))) \\
ATT_U &= f_{2dTCConv}(X) \otimes AM_U \\
Y &= (f_{2dTCConv}(ATT_U(f_{2dConv}(ATT_D(X)))) \\
&\quad + ATT_D(X)) + X
\end{aligned} \tag{9}$$

where $f_{2dTCConv}$ denotes the 2D transpose convolutional layer.

As shown in Fig. 6, S-GAPSCN consists of an encoder and a decoder. This encoder follows the same architecture as the encoder used in GAPSCN. By utilizing the RB as a first step in decoding, we are able to reconstruct the QPS and recover its original dimensions. Once the data dimension has been reconstructed, the MSSGAM is used to suppress the AWGN.

B. Comparing with Conventional Attention

In order to assess the relative effectiveness of different attention modules, we select the S-GAPSCN architecture as the basic architecture and train and test it by switching between simplified global attention and channel spatial (CS) attention [33]. The MSE and accuracy performance are presented in Table IV. Based on Table IV, simplified global attention achieves a superior MSE and accuracy for each CR when compared with the CS attention. Due to each bit in QPS is equally important and weighted, simplified global attention is able to capture more important information than the CS attention in the absence of pooling. In addition, simplified global attention can generate a joint channel spatial attention map, including the channel attention map and the spatial attention map. While the CS attention computes attention maps twice, one for channel attention and the other for spatial attention, simplified global attention only calculates attention maps once, implying that simplified global attention has a lower computational complexity than the CS attention. Based on the above observations, the simplified global attention module is expected to achieve a reliable reconstruction accuracy and a low computation complexity compared to the conventional attention module, which will be evaluated and verified in the following section.

V. EXPERIMENTAL STUDIES

A. Training Procedure

To train the GAPSCN and the S-GAPSCN, we use end-to-end training for all weights and biases by computing the loss. In the training state, we quantize the phase information using $K = 8$ bits. The training samples are taken as the input and the ground truth of the model. The noise will be added to

TABLE V
HYPERPARAMETER SETTINGS

| | |
|----------------|--------------------|
| Neurons | 64 |
| Batch size | 256 |
| Training epoch | 1000 |
| Learning rate | 10^{-4} |
| Optimizer | Adam |
| Loss function | Mean squared error |

the output of the encoder in the training stage. The training process is given by

$$\hat{\Theta} = f_{dec}(g \cdot f_{enc}(\Theta) + n), \tag{10}$$

where $\hat{\Theta}$ is the output of GAPSCN, and g is the constant channel coefficient [34] and n is the AWGN.

The loss function in training is characterized by the MSE, which can be expressed as

$$L = \frac{1}{M} \sum_{m=1}^M \|\hat{\theta}_m - \theta_m\|_2^2, \tag{11}$$

where $\hat{\theta}_m$ and θ_m represent the m -th column of $\hat{\Theta}$ and Θ , respectively. We chose the Adam algorithm [35] as the optimizer to update the parameters and the learning rate is 10^{-4} . The hyperparameter settings are summarized in Table. V.

B. Simulation Results and Analysis

The NMSE is adopted to demonstrate the prominent performance of the proposed GAPSCN and the S-GAPSCN, which can be formulates as

$$\text{NMSE} = \frac{\|\Theta - \hat{\Theta}\|_2^2}{\|\Theta\|_2^2}. \tag{12}$$

With the empirical results in [36], the training SNR we chose is 20dB, and the training epochs are 1000. Without loss of generality, we set the channel coefficient g to be 1. We generate training samples, validation samples, and test samples according to the uniform distribution. The sizes of training samples, validation samples, and test samples are 128000, 32000 and 128000, respectively.

For comparison, we consider the following convolutional attention-based compression methods including attention CsiNet [17] and SALDR [18] for performance comparison. The 2D convolutional layer in attention CsiNet and SALDR will switch to a 1D convolutional layer since our data type has one dimension, and other hyperparameter settings are the same as our proposed model. This is an ablation study of the effect of MSSGAM. In addition, we evaluate the model size and model complexity by calculating the number of parameters and examining the run time for the proposed S-GAPSCN.

The NMSE performance of the GAPSCN, S-GAPSCN, S-GAPSCN without MASSGN, Attention Csineti, SALDR and the PSCDN with CRs $\frac{1}{2}, \frac{1}{4}, \frac{1}{8}$ is shown in Fig. 8, Fig. 9 and Fig. 10, respectively. In Fig. 8, Fig. 9 and Fig. 10, the performance of all compression methods is increased with the increasing CR as expected. Furthermore, it is always found that the GPASCN achieves a superior NMSE performance

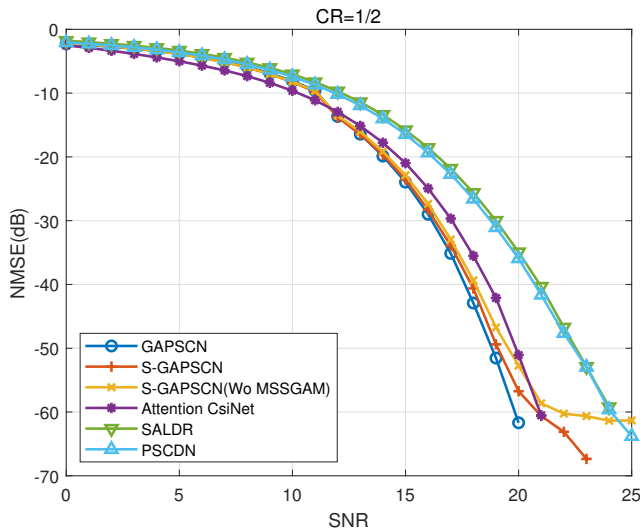


Fig. 8. NMSE performance (dB) comparison for different compression algorithms (attention CsiNet [17], SALDR [18] and PSCDN [7]) with $CR = \frac{1}{2}$.

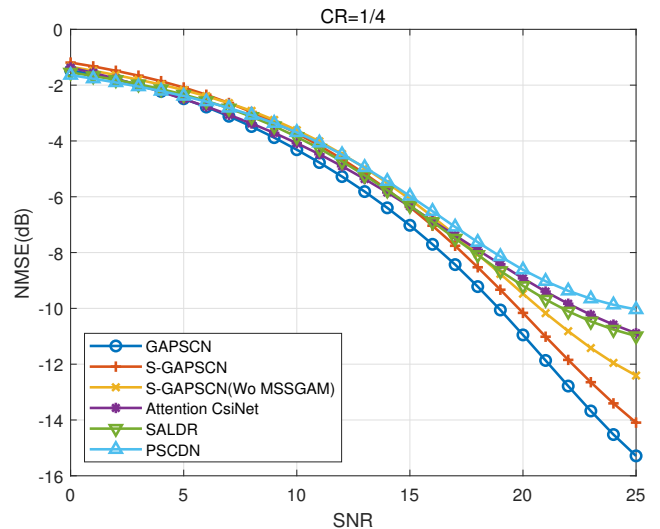


Fig. 9. NMSE performance (dB) comparison for different compression algorithms with $CR = \frac{1}{4}$.

TABLE VI
COMPUTATIONAL COMPLEXITY AND MODEL SIZE

| Model | Parameters | Processing time |
|------------------|------------|-----------------|
| GAPSCN | 290791 | 2.35s |
| S-GAPSCN | 91157 | 0.75s |
| Attention CsiNet | 2148670 | 1.55s |
| SALDR | 254660 | 2.47s |

when compared with two benchmark schemes for each CR, which can be explained by following modifications of the GAPSCN. First, by incorporating the missing correlated information between spatial and channel dimensions in the global attention, a more comprehensive attention map is established, in which more relevant information can be captured. Second, we abandon the pooling operation so that the information can be fully utilized. Last but not least, we rearrange the data distribution through the model utilizing the GND/IGDN layer. The MSSGAM significantly enhances the performance of S-GAPSCN as demonstrated in the ablation study results, which show S-GAPSCN outperforms S-GAPSCN without MSSGAM, and a small gap exists between S-GAPSCN and GAPSCN. The result is due to the fact that MSSGAM can capture critical information and mitigate the noise effect by using simplified global attention and multi-scale architecture.

In Table III, we compare the size and computational complexity of model decoders for different compression methods with a CR of $\frac{1}{8}$ and an SNR of 20dB. According to the results, S-GAPSCN has the least number of parameters and the fastest processing time. The S-GAPSCN demonstrates a prominent NMSE performance but with a low computational complexity.

VI. CONCLUSION

In this paper, we investigate and analyze the problem of feedback compression for the QPS in the IRS-assisted wireless system, by proposing a novel global attention-based model, namely, GAPSCN. In the proposed GAPSCN, we first supplant the missing correlated information between spatial and channel

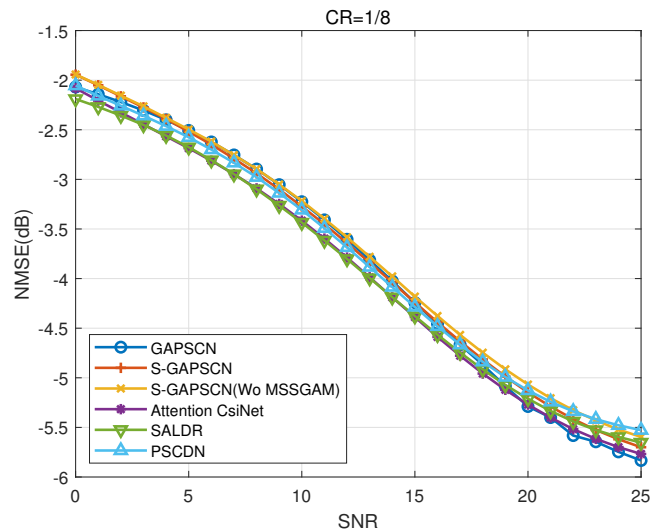


Fig. 10. NMSE performance (dB) comparison for different compression algorithms with $CR = \frac{1}{8}$.

dimensions in the global attention, and a more comprehensive attention map will be produced, which will allow the model to capture more crucial information. We then fully utilize the information by abandoning the pooling process. We further solve the problem of mismatched distribution by utilizing the GND/IGDN layer. Moreover, we propose S-GAPSCN to reduce the decoder complexity for the IRS, where the MSSGAM captures important information and mitigates the noise effect by utilizing a simplified global attention scheme and multi-scale architecture, respectively. Simulation results show that the proposed GAPSCN is capable of achieving an accurate reconstruction compared with existing algorithms, and S-GAPSCN provides almost equivalent performance but with a lower computational cost compared with GAPSCN.

REFERENCES

- [1] M. D. Renzo *et al.*, “Smart radio environments empowered by reconfigurable AI meta-surfaces: An idea whose time has come,” *EURASIP J. Wireless Commun. Netw.*, vol. 2019, no. 1, p. 129, May 2019.
- [2] Y. Liu, D. Li, B. Du, L. Shu, and G. Han, “Rethinking sustainable sensing in agricultural Internet of Things: from power supply perspective,” *IEEE Wireless Commun.*, 2022. doi: 10.1109/MWC.004.2100426.
- [3] Z. Gao, Y. Xu, Q. Wang, Q. Wu, and D. Li, “Outage-constrained energy efficiency maximization for RIS-assisted WPCNs,” *IEEE Commun. Lett.*, vol. 25, no. 10, pp. 3370–3374, Oct. 2021.
- [4] C. Pan, H. Ren, K. Wang, W. Xu, M. El-kashlan, A. Nallanathan, and L. Hanzo, “Multicell MIMO communications relying on intelligent reflecting surfaces,” *IEEE Trans. Wireless Commun.*, vol. 19, no. 8, pp. 5218–5233, Aug. 2020.
- [5] Y. Xu, Z. Gao, Z. Wang, C. Huang, Z. Yang, and C. Yuen, “RIS-enhanced WPCNs: Joint radio resource allocation and passive beamforming optimization,” *IEEE Trans. Veh. Technol.*, vol. 70, no. 8, pp. 7980–7991, Aug. 2021.
- [6] D. Li, “How many reflecting elements are needed for energy- and spectral-efficient intelligent reflecting surface-assisted communication,” *IEEE Trans. Commun.*, vol. 70, no. 2, pp. 1320–1331, Feb. 2022.
- [7] X. Yu, D. Li, Y. Xu and Y. -C. Liang, “Convolutional autoencoder-based phase shift feedback compression for intelligent reflecting surface-assisted wireless systems,” *IEEE Commun. Lett.*, vol. 26, no. 1, pp. 89–93, Jan. 2022.
- [8] M. H. Guo, T. X. Xu, J. J. Liu, Z. N. Liu, P. T. Jiang, T. J. Mu, S. H. Zhang, R. R. Martin, M. M. Cheng, and S. M. Hu, “Attention mechanisms in computer vision: A survey,” *Comp. Visual Media.*, vol. 8, no. 3, pp. 331–368, Sept. 2022.
- [9] M. Volodymyr *et al.*, “Recurrent models of visual attention,” in *Proc. Adv. Neural Inf. Process. Syst. (NIPS)*, 2014, pp. 2204–2212.
- [10] A. Vaswani *et al.*, “Attention is all you need,” in *Proc. Adv. Neural Inf. Process. Syst. (NIPS)*, 2017, pp. 6000–6010.
- [11] J. Hu, L. Shen and G. Sun, “Squeeze-and-excitation networks,” in *Proc. IEEE Conf. Comput. Vis. Pattern Recognit. (CVPR)*, 2018, pp. 7132–7141.
- [12] S. Woo, J. Park, J. g. Lee and I. S. Kweon, “CBAM: Convolutional block attention module,” in *Proc. Eur. Conf. Comput. Vis. (ECCV)*, 2018, pp. 1–17.
- [13] N. Vosco, A. Shenkler and M. Grobman, “Tiled squeeze-and-excite: Channel attention with local spatial context,” in *Proc. IEEE Int. Conf. Comput. Vis. Workshops (ICCVW)*, 2021, pp. 345–357.
- [14] D. Misra, T. Nalamada, A. U. Arasanipalai and Q. Hou, “Rotate to attend: Convolutional triplet attention module,” in *Proc. IEEE Winter Conf. Appl. Comput. Vis. (WACV)*, 2020, pp. 7936–7945.
- [15] Y. LeCun, K. Kavukcuoglu and C. Farabet, “Convolutional networks and applications in vision,” in *Proc. IEEE Int. Symp. Circuits Syst.*, 2010, pp. 253–256.
- [16] J. Ballé, V. Laparra, and E. P. Simoncelli, “Density modeling of images using a generalized normalization transformation,” in *Proc. Int. Conf. Learn. Represent. (ICLR)*, 2016, pp. 1–14.
- [17] Q. Cai, C. Dong and K. Niu, “Attention model for massive MIMO CSI compression feedback and recovery,” in *Proc. IEEE Wireless Commun. Netw. Conf. (WCNC)*, 2019, pp. 1–5.
- [18] X. Song *et al.*, “SALDR: Joint self-attention learning and dense refine for massive MIMO CSI feedback with multiple compression ratio,” *IEEE Wireless Commun. Lett.*, vol. 10, no. 9, pp. 1899–1903, Sept. 2021.
- [19] D. Li, “Ergodic capacity of intelligent reflecting surface-assisted communication systems with phase errors,” *IEEE Commun. Lett.*, vol. 24, no. 8, pp. 1646–1650, Aug. 2020.
- [20] D. Li, “Fairness-aware multiuser scheduling for finite-resolution intelligent reflecting surface-assisted communication,” *IEEE Commun. Lett.*, vol. 25, no. 7, pp. 2395–2399, Jul. 2021.
- [21] Goodfellow *et al.*, “Deep learning,” *MIT Press.*, 2015.
- [22] M. Abadi *et al.*, “TensorFlow: Large-scale machine learning on heterogeneous systems,” in <https://www.tensorflow.org/>, 2015.
- [23] Z. Cheng, H. Sun, M. Takeuchi and J. Katto, “Learned image compression with discretized Gaussian mixture likelihoods and attention modules,” in *Proc. IEEE Conf. Comput. Vis. Pattern Recognit. (CVPR)*, 2021, pp. 3138–3147.
- [24] K. He, X. Zhang, S. Ren, and J. Sun., “Deep residual learning for image recognition,” in *Proc. IEEE Conf. Comput. Vis. Pattern Recognit. (CVPR)*, 2016, pp. 770–778.
- [25] O. Ronneberger, P. Fischer, and T. Brox, “U-net: Convolutional networks for biomedical image segmentation,” in *Proc. Int. Conf. Med. Image Comput. Comput. Assist. Intervent.*, 2015, pp. 234–241.
- [26] F. Milletari, N. Navab, and S.-A. Ahmadi, “V-net: Fully convolutional neural networks for volumetric medical image segmentation,” in *Proc. IEEE Conf. Comput. 3D Vis. (3DV)*, 2016, pp. 565–571.
- [27] P. Liu, H. Zhang, W. Lian and W. Zuo, “Multi-level wavelet-CNN for image restoration,” in *Proc. IEEE Conf. Comput. Vis. Pattern Recognit. Workshops (CVPRW)*, 2018, pp. 886–895.
- [28] B. Park, S. Yu and J. Jeong, “Densely connected hierarchical network for image denoising,” in *Proc. IEEE Conf. Comput. Vis. Pattern Recognit. Workshops (CVPRW)*, 2019, pp. 2104–2113.
- [29] W. Liu, Q. Yan and Y. Zhao, “Densely self-guided wavelet network for image denoising,” in *Proc. IEEE Conf. Comput. Vis. Pattern Recognit. Workshops (CVPRW)*, 2020, pp. 1742–1750.
- [30] X. Jia, S. Liu, X. Feng and L. Zhang, “Focnet: A fractional optimal control network for image denoising,” in *Proc. IEEE Conf. Comput. Vis. Pattern Recognit. (CVPR)*, 2019, pp. 6047–6056.
- [31] L. Bao, Z. Yang, S. Wang, D. Bai and J. Lee, “Real Image denoising based on multi-scale residual dense block and cascaded u-net with block-connection,” in *Proc. IEEE Conf. Comput. Vis. Pattern Recognit. Workshops (CVPRW)*, 2020, pp. 1823–1831.
- [32] F. Jia, W. H. Wong and T. Zeng, “DDUNet: Dense dense u-net with applications in image denoising,” in *Proc. IEEE Int. Conf. Comput. Vis. Workshops (ICCVW)*, 2021, pp. 354–364.
- [33] Y. Zhang, K. Li, K. Li, G. Sun, Y. Kong and Y. Fu, “Accurate and fast image denoising via attention guided scaling,” *IEEE Trans. Image Process.*, vol. 30, pp. 6255–6265, Jul. 2021.
- [34] D. J. Love *et al.*, “An overview of limited feedback in wireless communication systems,” *IEEE J. Sel. Areas Commun.*, vol. 26, no. 8, pp. 1341–1365, Oct. 2008.
- [35] D. P. Kingma and J. L. Ba, “Adam: A method for stochastic optimization,” in *Proc. Int. Conf. Learn. Represent. (ICLR)*, 2015, pp. 1–15.
- [36] J. Guo *et al.*, “Convolutional neural network-based multiple-rate compressive sensing for massive MIMO CSI feedback: Design, simulation, and analysis,” *IEEE Trans. Wireless Commun.*, vol. 19, no. 4, pp. 2827–2840, Apr. 2020.